

FINAL TECHNICAL REPORT:
Award Number 02HQGR0120
FAULT LOADING PROCESSES IN THE NEW MADRID
SEISMIC ZONE

September 26, 2005

Paul Segall
(650-723-7241, segall@stanford.edu)
Geophysics Department
Stanford University
Stanford, CA 94305-2215

1 Technical Abstract

Our understanding of the tectonic processes which generate intraplate earthquakes such as in the New Madrid seismic zone is severely limited. There are, as yet, no widely agreed upon mechanical models for such earthquakes. In this project we developed tectonically reasonable models for the generation of intraplate earthquake sequences. In one set of numerical experiments we used the Finite Element Method (FEM) to examine the effects of glacial unloading on stressing intraplate faults. In a second set of numerical experiments we used rate and state dependent friction laws to study intraplate earthquakes that might be induced by the post glacial rebound stresses.

2 Stressing due to glacial unloading

Due to the presence of an initial stress field in the Earth, the equations governing stress and displacement in a viscoelastic, layered medium in response to a surface load are usually expressed as perturbations from a pre-existing equilibrium state. The necessary equations are the incremental momentum balance, the incremental continuity equation and the incremental constitutive equation. Most finite element packages correctly handle the continuity and constitutive equations and we will therefore not consider these here.

The material incremental momentum equation for quasi-static, infinitesimal perturbations of a stratified, compressible, fluid Earth initially in hydrostatic equilibrium subject to gravitational forces

but neglecting inertial forces is

$$\sigma_{ij,j}^{\delta} + (p_{,j}^0 u_j)_{,i} + \rho^{\Delta} g_i^0 + \rho^0 g_i^{\Delta} = 0 \quad (1)$$

where σ is the Cauchy stress tensor defined as positive in tension, $p = -\sigma_{kk}/3$ is the pressure, ρ the density, g the gravitational acceleration and u the displacement. The superscripts 0, δ and Δ denote the initial, material incremental and local incremental fields respectively. The usual summation and differentiation conventions apply to the index notation. The first term in Eq. 1 describes the force from spatial gradients in stress. The second term concerns the incremental stress resulting from a particle's displacement in the initial stress field, parallel to the stress gradient. This term is commonly referred to as "pre-stress advection". The third and fourth term describe perturbations to the gravitational forces due to changes in density and gravitational acceleration, respectively. The third term is sometimes referred to as the buoyancy term, which, together with the second term, accounts for isostasy.

The momentum equation is frequently simplified by ignoring the change in the gravitational field within, that is neglecting the fourth term which is insignificant except at the very longest wavelengths. A model with this approximation is described as non-self-gravitating. Further simplification is obtained for a layer that is uniform in density and incompressible, since the third term in Eq. 1 vanishes. For a non-self-gravitating incompressible uniform Earth the momentum equation can be rewritten in terms of the local incremental stress as

$$\sigma_{ij,j}^{\Delta} = 0 \quad (2)$$

$$\sigma_{ij}^{\Delta} = \sigma_{ij}^{\delta} + p_{,k}^0 u_k \delta_{ij} = \sigma_{ij}^{\delta} + \rho^0 g^0 u_k \delta_{ij} \quad (3)$$

We used this simplified equation for the finite element modeling.

2.1 Implementation of the viscoelastodynamic equations into Finite Element codes

We are indebted to Prof. P. Wu for invaluable help on the implementation of the simplified viscoelastodynamic momentum equation into Abaqus, our commercial finite element analysis package. The following paragraphs are based on discussions with, and a manuscript by, Prof. Wu.

Most commercial finite element packages are mainly designed for engineering applications where only the divergence of the stress tensor is included in the momentum equation, $S_{ij,j} = 0$, ignoring isostasy and self-gravitation. This makes the modeling codes unsuitable for geophysical applications involving long wavelengths and non-elastic deformation [13]. If we, however, consider our model as non-self-gravitating and the elements as incompressible and uniform in density, we can utilize Eqs. 2 and 3 to define a new, finite element stress tensor as

$$\mathbf{S}^{\text{FE}} = \mathbf{S} - \rho^0 g^0 u_z \mathbf{I} \quad (4)$$

where u_z is the displacement in the vertical direction, parallel to the gravity field, and \mathbf{I} is the identity matrix. Differentiation gives us

$$S_{ij,j}^{\text{FE}} = S_{ij,j} - \rho^0 g^0 u_{z,j} \delta_{ij} = 0 \quad (5)$$

which is the momentum equation we desire, expressed in terms of the new stress. Due to the transfor-

mation in Eq. 4, new boundary conditions must be applied to the finite elements. In the following, P is the surface load, the index h signifies a horizontal coordinate and $[F]_{Z-}^{Z+} = \lim_{\epsilon \rightarrow 0} (F(Z+\epsilon) - F(Z-\epsilon))$.

1. At the Earth's surface: $S_{zz}^{\text{FE}} + \rho^0 g^0 u_z]_{z=0} = P$, assuming the density of air to be zero, and $S_{hz}^{\text{FE}}]_{z=0} = 0$
2. At solid-solid interfaces at depth Z : $[S_{zz}^{\text{FE}}]_{Z-}^{Z+} = (\rho_+ - \rho_-)g^0 u_z$ and $[S_{hz}^{\text{FE}}]_{Z-}^{Z+} = [u_h]_{Z-}^{Z+} = [u_z]_{Z-}^{Z+} = 0$

These boundary conditions are easily implemented in finite element packages as Winkler, or elastic, foundations with spring constants $\rho^0 g^0$ or $(\rho_+ - \rho_-)g^0$, respectively. All non-vertical material interfaces should have these foundations attached.

Finally, due to the transformation in Eq. 4, the stress output after a finite element model run has to be converted back to the ‘‘correct’’ stress through $\mathbf{S} = \mathbf{S}^{\text{FE}} + \rho^0 g^0 u_z \mathbf{I}$. This conversion is crucial since stress magnitudes otherwise will be much too low. Displacements in the finite element model are not affected by the transformation and, therefore, need no postprocessing.

2.2 Benchmark tests of the Finite Element implementation

We implemented the Winkler foundation formalism discussed above in our finite element package Abaqus and performed a number of benchmark tests. Three of these tests will be discussed below. Our models below all have an interior area of good resolution approximately 2500x2000 km, increasing element size away from the interior out to 10000x5000 km and infinite elements to the sides and at the bottom. The models have not been optimized for efficiency or accuracy, we have simply used models that seem ‘‘big enough’’.

2.2.1 Viscoelastic half-space in 2D with a boxcar Heaviside load

The solution for the response of a viscoelastic half-space to an impulsive boxcar load with uniform amplitude is well known, e.g. [11]. The vertical displacement at the surface is given in the wave-number domain by

$$\int_{-\infty}^{\infty} \frac{-PL(k)}{\rho g + 2\mu k} \left[1 + \frac{2\mu k}{\rho g} (1 - e^{-\alpha t}) \right] e^{ikx} dk \quad (6)$$

where P is the amplitude of the boxcar load and $L(k)$ its wave-number k domain representation. α is the relaxation time given by

$$\alpha = \frac{\rho g \mu}{\eta(\rho g + 2\mu k)} \quad (7)$$

We evaluated Eq. 6 numerically using a Fast Fourier Transform (FFT) and compared our finite element calculations to the FFT result. Figure 1 shows the comparison of the two methods for a 15 MPa 2D boxcar load with 1000 km half-length applied to a 2D, incompressible, non-self-gravitating viscoelastic half-space with the following parameters:

Density	5000 kg/m ³
Young's modulus	113 GPa
Viscosity	1.45 × 10 ²¹ Pa s
Poisson's ratio	0.5
Gravity	9.82 m/s ²

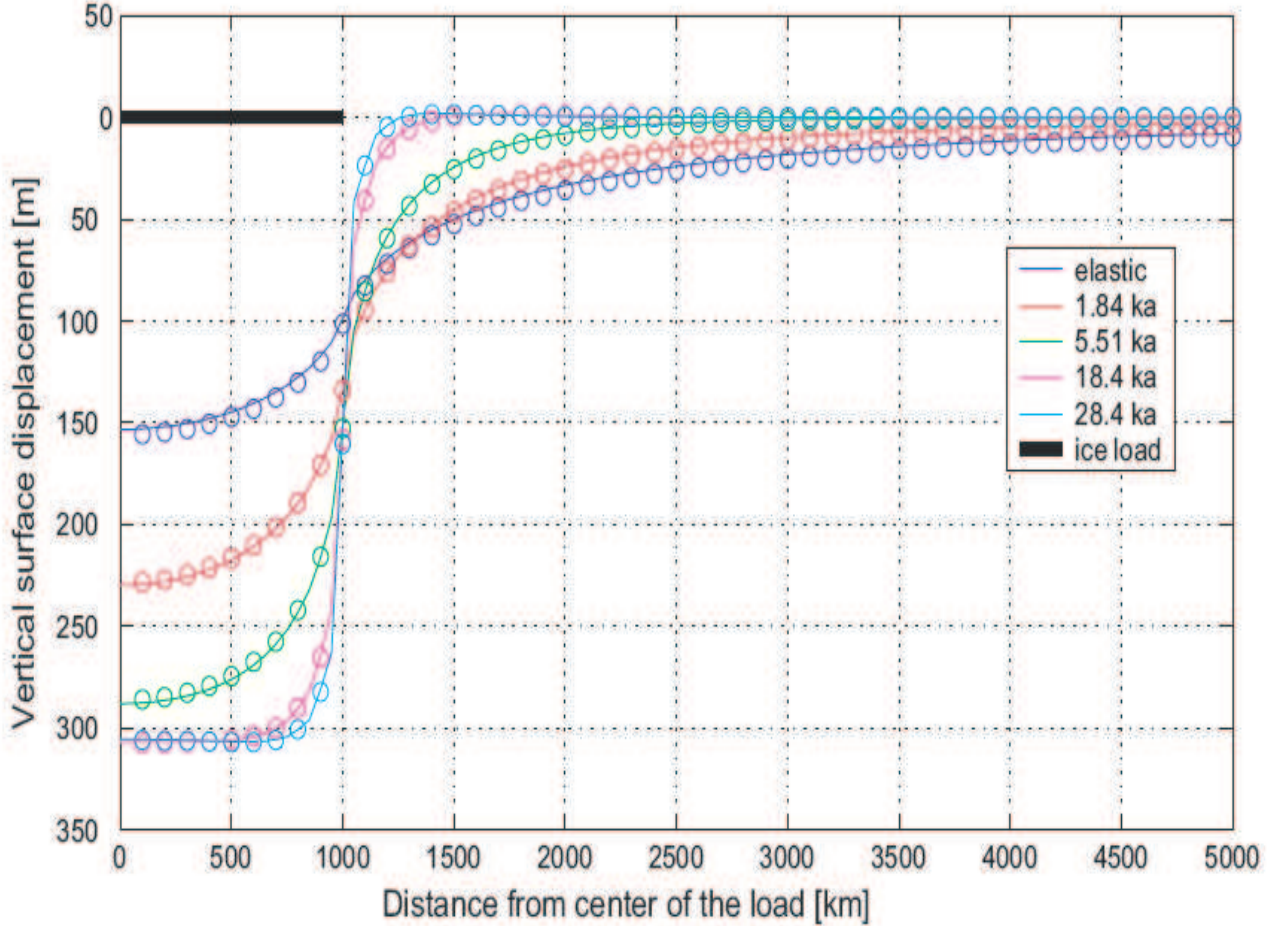


Figure 1: Vertical surface displacement of a viscoelastic half-space subject to a Heaviside load. Lines are finite element modeling results and circles are results from the transform method. Times are in 1000 years after the application of the load.

As Figure 1 shows, the two methods agree extremely well for the vertical surface displacements. Our results also agree well with the finite element calculations of [14], for a similar 2D model, both in terms of vertical surface displacements and Mises stress.

We compared our finite element model of an axisymmetric viscoelastic half-space subject to an impulsive boxcar load with the finite element model of [15]. The results for vertical surface displacements agree very well, although the comparison in this case was visual rather than numerical.

We tested our finite element implementation against the transform method results of [5]. The tested model is an axisymmetric model with an elastic plate overlying a viscoelastic half-space. The model is subjected to an ice load of elliptic cross-section, 2.8 km high at the center with a density of 0.91 kg/m^3 . The loading history is a simplified representation of the final Weichselian glaciation in Fennoscandia, the load is linearly increased over 90 kyr to its maximum, referred to as the Last Glacial Maximum (LGM), and then linearly decreased to zero over 10 kyr, End of Glaciation (EoG). The model is run for an additional 8 kyr up to current times. Parameters of the model are:

Layer	1	Half-space
Density	3380	3380 kg/m^3

Young's modulus	192	435 GPa
Viscosity	∞	1.0×10^{21} Pa s
Poisson's ratio	0.5	0.5
Gravity	9.81	9.81 m/s^2

We also compared the results of our FEM calculations with the calculations of [5], and find the results are remarkably similar. Maximum shear stress contours agree both in shape and numerically and the stress states are very similar, although not identical. This could be due to the algorithm used to evaluate the state of stress, and also to the relative isotropy of the stress state in parts of the model.

3 Modeling of Intraplate Faults with Rate and State Dependent Friction Laws

We used the rate and state friction framework to study intraplate earthquakes. Rate and state friction laws, developed to incorporate experimental observations [Dieterich, 1979, 1981; Ruina, 1983], model the variations of frictional shear strength due to its dependence on slip rate and on the evolving population of asperity contacts. The laws have been successfully used to explain various aspects of stable and unstable sliding between elastic solids, and to model earthquake phenomena, including nucleation, earthquake slip, spatiotemporal complexities in slip, and aftershocks.

A general class of friction constitutive laws relates the shear stress τ , effective normal stress σ , slip rate V , and the state of asperity contacts, which is assumed to be suitably described by one state variable θ . Developed to explain laboratory observations, the rate and state constitutive laws can be formulated as follows

$$\tau = \psi(\sigma, V, \theta) = \bar{\sigma} \hat{\psi}(V, \theta) \quad (8)$$

$$d\theta/dt = \varphi(V, \theta) \quad (9)$$

where $\hat{\psi}(V, \theta)$ is the friction coefficient, $\bar{\sigma}$ is effective normal stress, and τ , V , and θ depend on space variables and time. Different rate and state constitutive laws have been formulated to model laboratory observations of rock friction based on the selection of $\hat{\psi}(V, \theta)$ and $\varphi(V, \theta)$. The most commonly used friction relation is

$$\tau = \bar{\sigma} [\mu_0 + a \ln(\frac{V}{V_0}) + b \ln(\frac{V_0 \theta}{L})] \quad (10)$$

where V_0 is a reference velocity, μ_0 is the steady-state friction at $V = V_0$, a and b are material properties, and L is the critical slip distance (can be interpreted as a characteristic slip distance required for evolution to the steady state, sometimes denoted by or D_c or d_c). We use the so-called slowness form of the state evolution equation

$$d\theta/dt = 1 - \frac{\theta V}{L} \quad (11)$$

Here, θ is interpreted as a characteristic lifetime of the asperity population on the contact surfaces; L is then interpreted as a measure of the sliding distance required to establish a new population of asperity contacts (and hence is assumed to be independent of V).

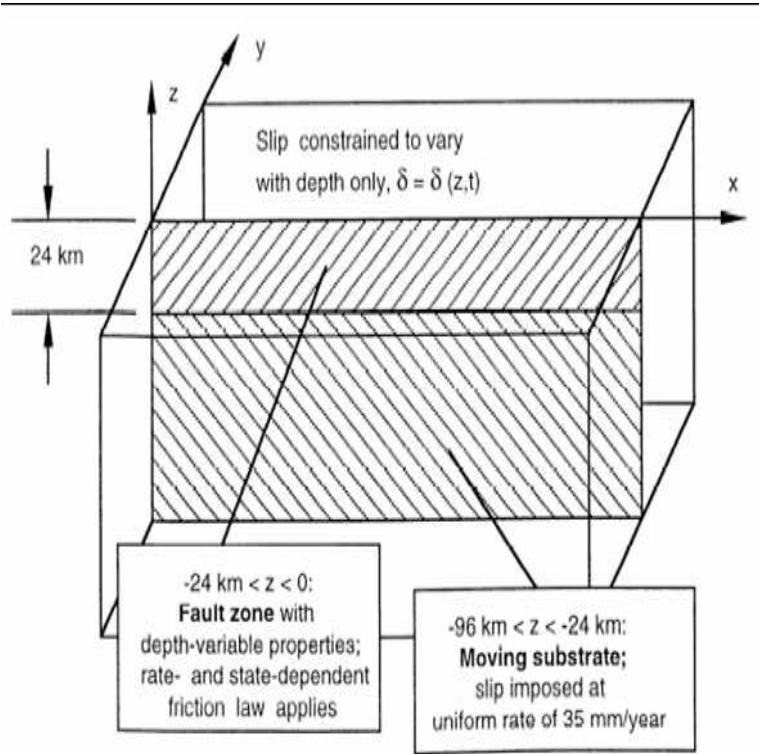


Figure 2: 2-D vertical strike-slip fault in an elastic half-space

If the slip velocity V is suddenly increased or decreased, the stress τ simultaneously increases or decreases. If slip velocity V is held constant, the stress τ monotonically evolves toward a new steady-state value given by

$$\tau = \bar{\sigma} [\mu_0 + (a - b) \ln(\frac{V}{V_0})] \quad (12)$$

3.1 2-D Anti-Plane Spectral Formulation

In this study, we used a code modified from the 2-D anti-plane spectral formulation developed by [6]. Figure 2 outlines the 2-D model used in [6]. In their model, a vertical strike-slip fault with depth-variable properties is embedded in an elastic half-space. The fault is driven below 24 km by steady slip at a plate rate of 35 mm/yr. In the shallower zone, where rate and state friction applies, the slip is calculated as a function of depth and time. For more detail about this model, refer to [6].

This model well describes plate boundary settings, where relative far-field velocities equal the deep interseismic slip rate that drive earthquakes at shallower depths. However, it is not appropriate for intraplate regions such as the New Madrid Seismic Zone, where relative motions in the far field are zero.

To properly understand the mechanics of intraplate earthquakes, we modify Lapusta et al.'s [2000] code. We extend the velocity-strengthening region from 14 km to 96 km.

need to explain that this is a way to simulate the finite length effects in the 2D context. The earthquakes are triggered by the stress accumulation in the velocity-weakening region due to the shear stresses applied at the lateral remote boundaries which are proxies for the effects of post-glacial loading. Stresses released by an earthquake in the velocity-weakening region will accelerate creep in the velocity-strengthening region. Additional creep in the deeper velocity-strengthening

region, in return, partially reload the upper crust, leading to cyclic stress transfer in the manner originally proposed by [Kenner and Segall] . Our numerical experiments were designed to simulate the generation of repeated large intraplate earthquakes. In particular, we wished to determine how the number of earthquakes and their temporal distribution depend on the amplitude of the imposed stress perturbation.

The simulations of intraplate earthquakes proceed as follows:

- Start with some reasonable initial conditions, run Lapusta’s cycle model code generating a numerical earthquake sequence.
- Decrease the remote plate velocity to zero, and continue the computations. Without stressing due to plate boundary motion the number of model earthquakes decreases dramatically. We stop the calculation when the simulated earthquakes in the upper 15 km or so become relatively rare.
- Impose a stress step to simulate the effects of glacial unloading, and observe what happens.

To better understand the numerical results, we consider the time evolution of creep in the velocity-strengthening region beneath the seismogenic zone. We assume this region slips at near steady state friction, as given by (12). With a locked seismogenic fault, the creeping zone acts like a crack of length l . We estimate for creep to accumulate slip equal to that in a large intraplate earthquake. This does not guarantee that an earthquake will nucleate at this time, but gives a rough feeling for how long it takes to load the fault to failure.

From elastic crack theory

$$\tau = \tau_0 - \alpha u \quad (13)$$

where τ_0 is the initial shear stress in the infinity, $\alpha = G/2l$ and G is shear modulus. Combining equations (13) and (12) and ignoring spatial variations in slip, slip on the creeping fault is governed by

$$\frac{du}{dt} = V_0 \exp\left(\frac{\tau_0 - \mu_0 \sigma - \alpha u}{A}\right) \quad (14)$$

where $A = \sigma(a - b)$. The solution to this differential equation given initial condition $u(0) = 0$, is

$$u = \frac{A}{\alpha} \ln\left[\frac{\alpha}{A} V_0 t + \exp\left(\frac{\sigma \mu_0 - \tau_0}{A}\right)\right] + \frac{\tau_0 - \sigma \mu_0}{\alpha} \quad (15)$$

Thus, displacement accumulates logarithmically in time. We can use this to estimate, given an initial stress, how long it takes for 5 m of slip to accumulate. Solving for time

$$t = \frac{A}{\alpha V_0} \exp\left(\frac{\sigma \mu_0 - \tau_0}{A}\right) \left[\exp\left(\frac{\alpha u}{A}\right) - 1\right] \quad (16)$$

From the slip we can compute the stress acting on the creeping part of the fault

$$\tau = \sigma \mu_0 - A \ln\left[\frac{\alpha}{A} V_0 t + \exp\left(\frac{\sigma \mu_0 - \tau_0}{A}\right)\right] \quad (17)$$

In the numerical experiments described below, we find that the stress decays logarithmically due to creep, as predicted.

We start with initial conditions illustrated in Figure 3. The depth distribution of the constitutive parameters a , b and D_c are the same as used in Lapusta et al.’s [2000]. The effective normal stress

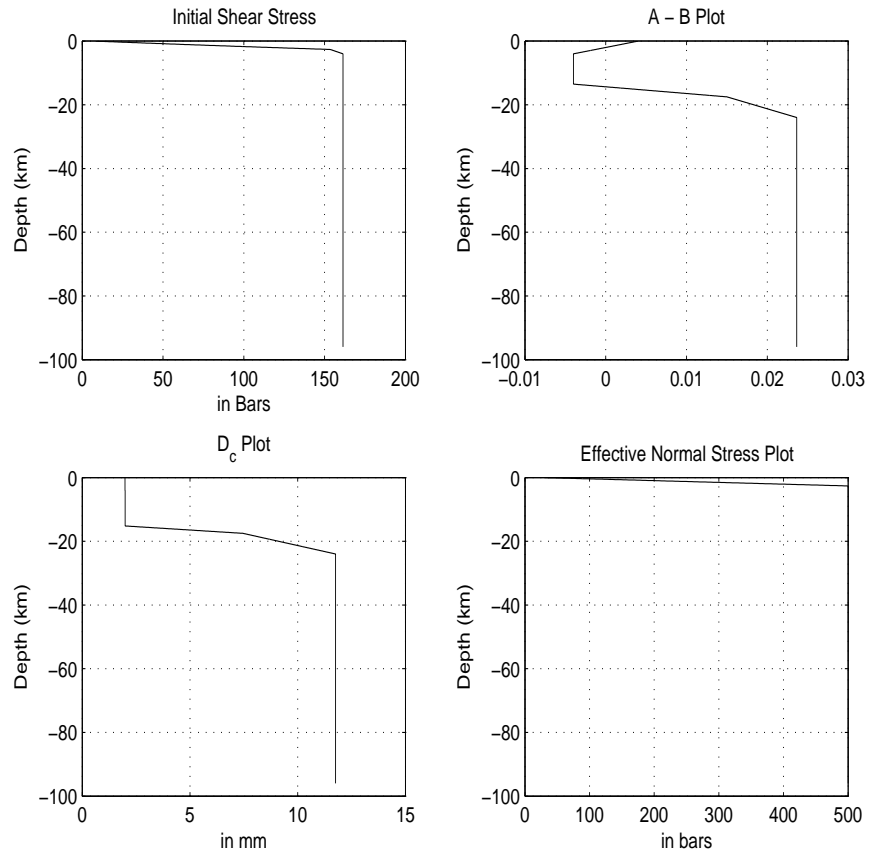


Figure 3: Initial conditions. a) shear stress, b) a-b, c) d_c , d) normal stress.

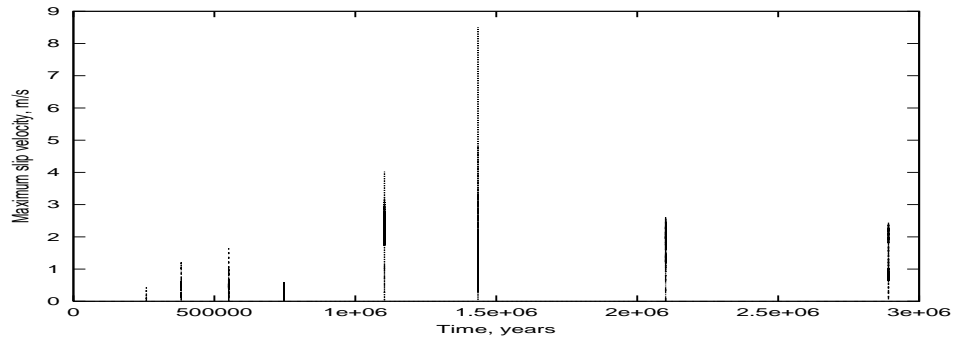


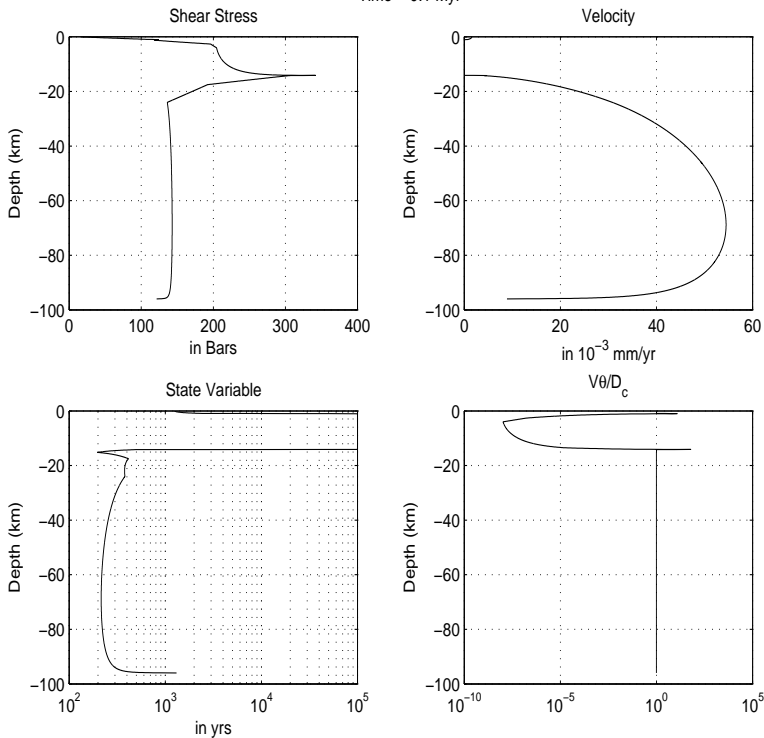
Figure 4: Maximum slip velocity (m/s) as a function of time (yr)

$\bar{\sigma} = \min[2.8 + (18z/\text{km}), 50]$. We take the initial shear stress τ_0 to be ~ 160 bars. If τ_0 is too small, it takes a long time to generate a sequence of earthquakes. If τ_0 is too large, earthquakes occur too frequently.

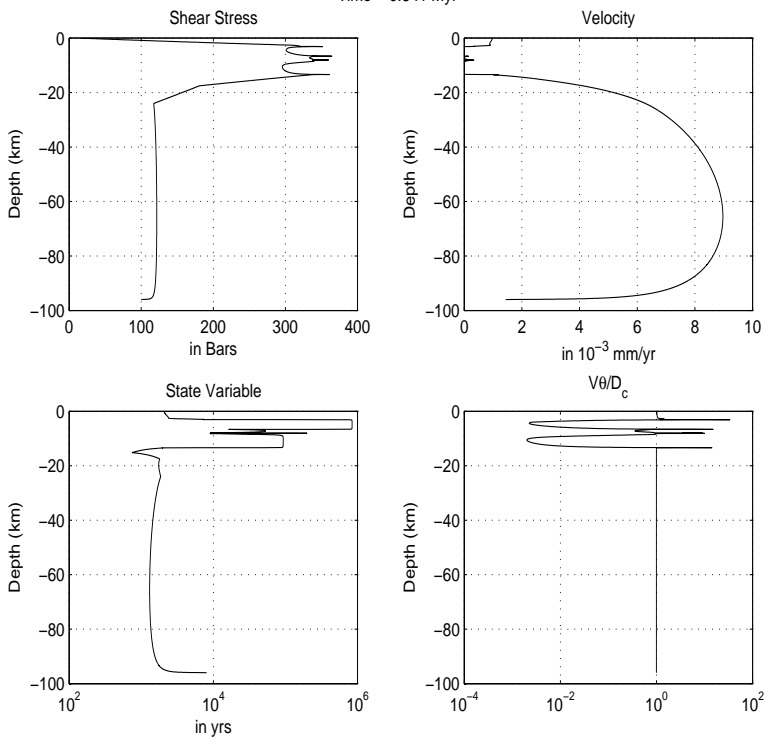
Figure 4 illustrates the maximum slip speed on the fault as a function of time. The spikes in slip-rate represent simulated earthquakes. The first event occurs at ~ 0.26 Myrs. Figures 5 and 6 show the shear stress, velocities, state variable, and $V\theta/D_c$ as functions of depth at selected times: $t=0.1, 0.841, 1.410, 1.647,$ and 1.749 Myrs, illustrating how these variables evolve with time.

Between 1.5 Myrs and 1.78 Myrs, there are relatively few simulated earthquakes. We take this as a reasonable initial condition for the simulation of stressing due to glacial rebound. In the following experiments, we imposed stress perturbations at time 1.647 Myrs.

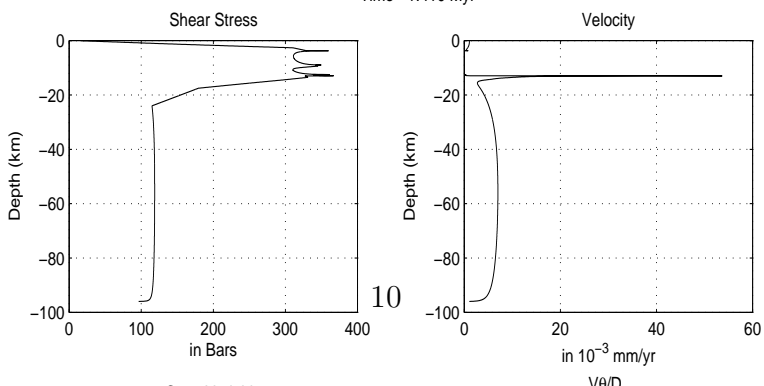
Time = 0.1 Myr



Time = 0.841 Myr



Time = 1.410 Myr



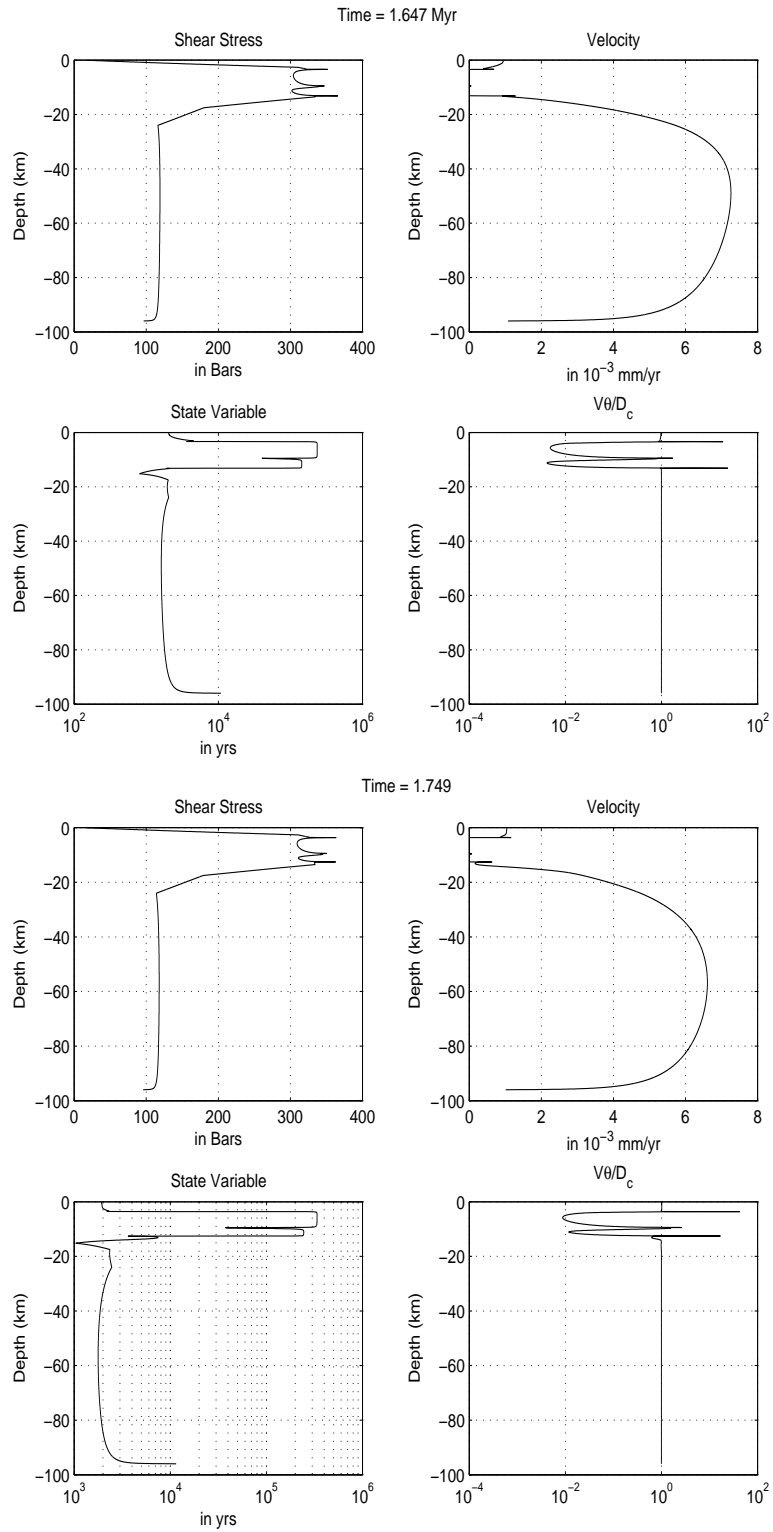


Figure 6: The shear stress, velocities, state variable, and $V\theta/D_c$ as functions of depth at time 0.1, 0.841, 1.410, 1.647, and 1.749 Myrs

To test the impact of the magnitude of the stress perturbation, we examined perturbations of: 1 mpa, 1.5 mpa, 1.8 mpa, 2.0 mpa, 2.5 mpa, and 3 mpa, all from the same initial conditions at 1.647 Myrs (see Figure 6 for the parameters). Figure 8 and 9 shows the sequence of events following the perturbation.

Following the 1 Mpa perturbation, there are two events within 0.1 Myr with the first event at ~ 700 yrs after the perturbation. With increasing magnitude of the perturbing stress, the events occur more frequently in time. In addition the first event happens closer in time to the perturbation. With a 3 MPa perturbation, there are 17 events (because of the plot scale, figure 9 does not show all the 17 events) within 100,000 years, with the first event ~ 300 yrs after the imposed stress perturbation.

The shear stress, slip rate, state variable, and $V\theta/D_c$ are shown as a function of depth right before and after an event with 1 MPa perturbation are show in Figure 10. We observe that in the shallow, velocity-weakening fault, immediately before the earthquake, shear stress accumulated to ~ 450 bars with significant stress drop during the earthquake. The coseismic slip partially reloads in the deep creeping fault causing stress transfer back to the seismogenic fault.

The numerical experiments show that modest shear stress perturbations due to e.g., post-glacial loading could produce a sequence of earthquakes. More work is needed to more thoroughly understand this model and to compare to observations.

References

- [1] Dieterich, J. H., Modeling of rock friction, 1. Experimental results and constitutive equations, *J. Geophys. Res.*, *84*, 2161-2168, 1979.
- [2] Dieterich, J. H., Constitutive properties of faults with simulated gouge, in *Mech. Behavior Crustal Rocks*, edited by N. L. Carter et al, *Geophys. Monogr. Ser.*, *24*, pp. 103-120, AGU, Washington, D.C., 1981.
- [3] Johnston, P., P. Wu and K. Lambeck, Dependence of horizontal stress magnitude on load dimension in glacial rebound models. *Geophys. J. Int.*, **132**, 41–60, 1998.
- [4] Kenner, S. J., and P. Segall, A mechanical model for intraplate earthquakes: application to the New Madrid Seismic Zone, *Science*, *289*, 2329-2332, 2000.
- [5] Klemann, V. and D. Wolf, Modelling of stresses in the Fennoscandian lithosphere induced by Pleistocene glaciations. *Tectonophysics*, **294**, 291–303, 1998.
- [6] Lapusta, N., J. R. Rice, Y. Ben-Zion, G. Zheng, Elastodynamic analysis for slow tectonic loading with spontaneous rupture episodes on faults with rate- and state-depedent friction, *J. Geophys. Res.*, *105*, 23,765-23,789, 2000.
- [7] Liu, L., M. D. Zoback, and P. Segall, Strain accumulation in the New Madrid seismic zone, *Science*, *257*, 1,666-1,669, 1992.
- [8] Newman, A., S. Stein, J. Weber, J. Engeln, A. Mao, and T. Dixon, Slow deformation and lower seismic hazard at the New Madrid Seismic Zone, *Science*, *284*, 619-621, 1999.
- [9] Ruina, A. L., Slip instability and state variable friction laws, *J. Geophys. Res.*, *88*, 10,359-10,370, 1983.

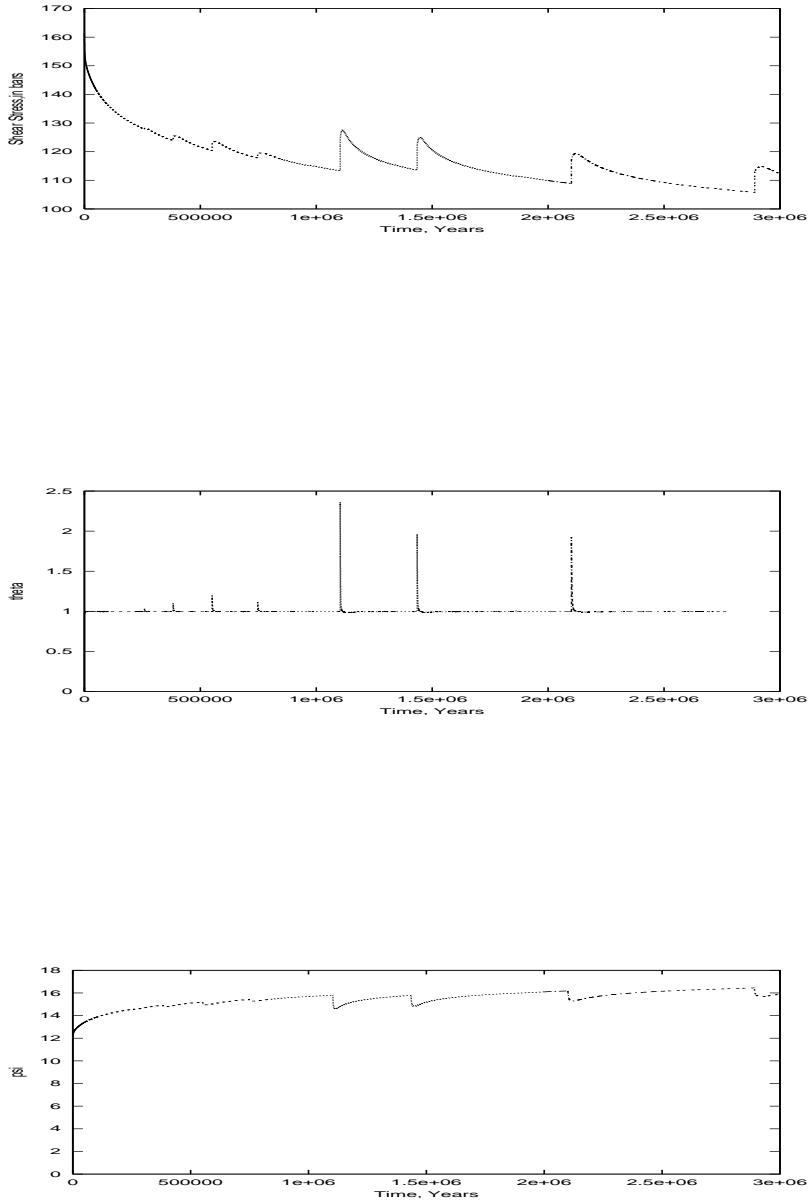


Figure 7: The evolution of shear stress τ , state variable θ and $\phi = \ln(V_0\theta/L)$ at depth 24 km

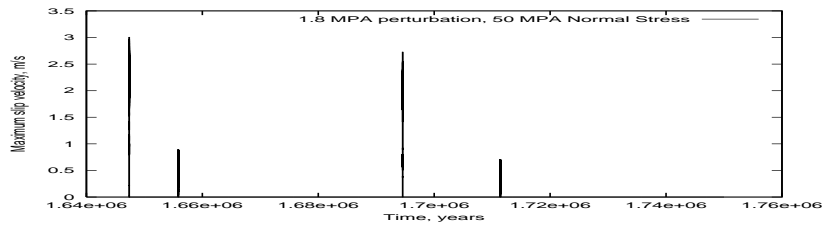
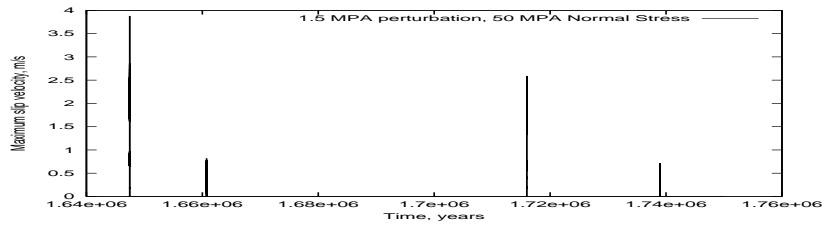
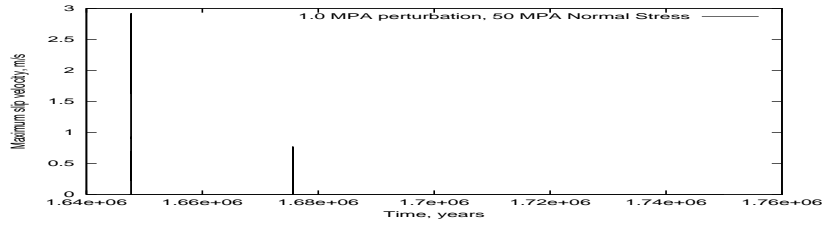


Figure 8:

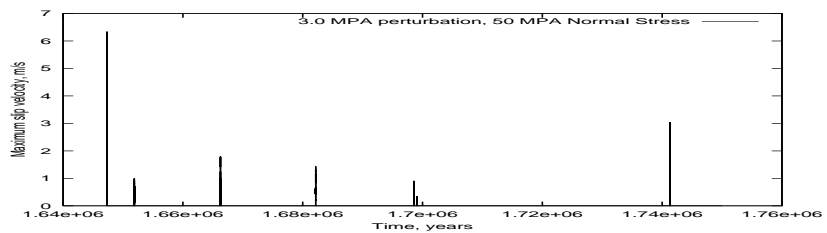
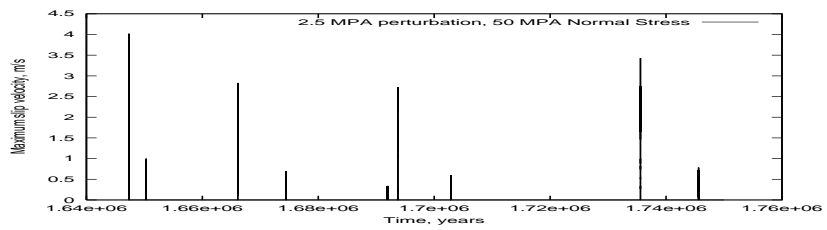
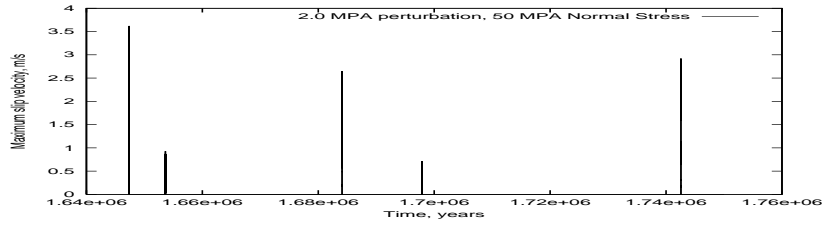


Figure 9: Maximum slip velocity (m/s) as a function of time (yr) with different magnitude of perturbation: 1.0, 1.5, 1.8, 2.0, 2.5, and 3.0 mpa at time 1.647 Myrs

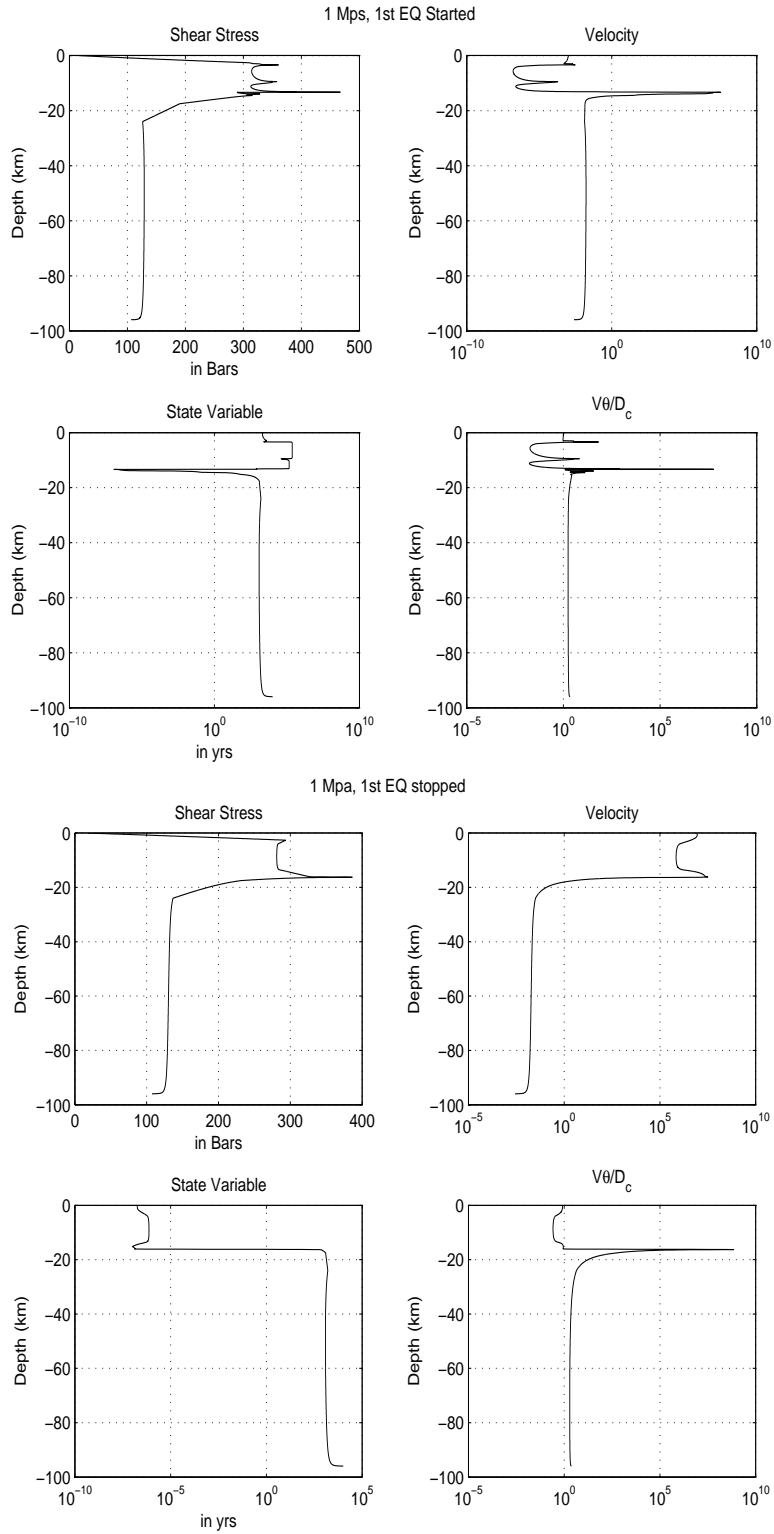


Figure 10: Maximum slip velocity (m/s) as a function of time (yr) right before and after the first event with 1mpa perturbation at time 1.647 Myrs

- [10] Weber, J., S. Stein, and J. Engeln, Estimation of strain accumulation in the New Madrid seismic zone from GPS geodesy, *Tectonics*, **17**, 250-266, 1998.
- [11] Wolf, D., On Boussinesq's problem for Maxwell continua subject to an external gravity field. *Geophys. J. R. astr. Soc.*, **80**, 275–279, 1985.
- [12] Wolf, D., Viscoelastodynamics of a stratified, compressible planet: incremental field equations and short- and long-time asymptotes. *Geophys. J. Int.*, **104**, 401–417, 1991.
- [13] Wu, P., Viscoelastic versus viscous deformation and the advection of pre-stress. *Geophys. J. Int.*, **108**, 136–142, 1992.
- [14] Wu, P., Deformation of an incompressible viscoelastic flat earth with power-law creep: a finite element approach. *Geophys. J. Int.*, **108**, 35–51, 1992.
- [15] Wu, P., Postglacial rebound in a power-law medium with axial symmetry and the existence of the transition zone in relative sea-level data. *Geophys. J. Int.*, **114**, 417–432, 1993.

Non-Technical Abstract

Our understanding of the tectonic processes which generate intraplate earthquakes such as those in the New Madrid seismic zone is severely limited. There are, as yet, no widely agreed upon mechanical models for such earthquakes. In this project we using numerical computer simulations to developed tectonically reasonable models for the generation of intraplate earthquake sequences. In one set of experiments we examined the effects of the retreat of the last glacial ice sheet on stressing of faults in the New Madrid region. In a second set of numerical experiments we applied laboratory derived friction laws to study how intraplate faults respond to stresses induced by post glacial rebound.